

Bayesian mixed model inference for genetic association under related samples with brain network phenotype

Xinyuan Tian^{1,†}, Yiting Wang^{1,†}, Selena Wang¹, Yi Zhao², Yize Zhao¹

¹Department of Biostatistics, Yale University, New Haven, CT

²Department of Biostatistics and Health Data Science,
Indiana University School of Medicine, Indianapolis, IN

Abstract

Genetic association studies for brain connectivity phenotypes have gained prominence due to advances in non-invasive imaging techniques and quantitative genetics. Brain connectivity traits, characterized by network configurations and unique biological structures, present distinct challenges compared to other quantitative phenotypes. Furthermore, the presence of sample relatedness in most imaging genetics studies limits the feasibility of adopting existing network-response modeling. In this paper, we fill this gap by proposing a Bayesian network-response mixed-effect model that considers a network-variate phenotype and incorporates population structures including pedigrees and unknown sample relatedness. To accommodate the inherent topological architecture associated with the genetic contributions to the phenotype, we model the effect components via a set of effect subnetworks and impose an inter-network sparsity and intra-network shrinkage to dissect the phenotypic network configurations affected by the risk genetic variant. To facilitate uncertainty quantification of signaling components from both genotype and phenotype sides, we develop a Markov chain Monte Carlo (MCMC) algorithm for posterior inference. We evaluate the performance and robustness of our model through extensive simulations. By further applying the method to study the genetic bases for brain structural connectivity using data from the Human Connectome Project with excessive family structures, we obtain plausible and interpretable results. Beyond brain connectivity genetic studies, our proposed model also provides a general linear mixed-effect regression framework for network-variate outcomes.

Keywords: Brain connectivity; Genome-wide association studies; Imaging genetics; Matrix-variate; Mixed effects; Network-response model; Sample relatedness.

[†] Equally contributed

1 Introduction

Brain imaging genetics, aiming to uncover the genetic basis of brain structure and function, has provided an unprecedented opportunity to understand the molecular support for different neurobiological processes (Shen and Thompson, 2020). By leveraging imaging quantitative traits as endophenotypes that reflect underlying neurological etiologies, we gain a deeper understanding of the risk biomarkers implicated in both disease outcomes and normal trajectory of development and aging (Ramasamy et al., 2014b; Zhao et al., 2021b).

Brain connectivity, encoding the relations between distinct units or nodes within a nervous system, has played an essential role in disclosing the brain neuronal interactions and reflecting correspondence with behavior. Depending on the aspect of characterization, brain connectivity can be summarized by anatomical links capturing the white matter fiber tracts known as structural connectivity, or statistical dependence between functional time courses known as functional connectivity. Converging evidence indicates brain connectivity is heritable, and can offer distinct genetic underpinnings compared with other neuroimaging traits (Zhao et al., 2021a; Elliott et al., 2018). This underscores the significance of studying the genetic contributions to connectivity patterns. From an analytical perspective, structural and functional connectivity can be viewed as an undirected graph with all the nodes over the brain as the vertex set and the corresponding connections as the edge set. By extracting single edges as univariate phenotypes, most of the current genome-wide association

studies (GWAS) were performed separately on each brain connection (Zhao et al., 2021a; Jahanshad et al., 2013; Elsheikh et al., 2020). However, such analyses overlook the biological interdependence and graphical structure inherent in brain network topography, which can raise concerns regarding biological plausibility and interpretability, as our data application demonstrates. In addition, this type of univariate approach finishes with a step of accounting for multiplicity, which significantly reduces the statistical power.

On the other hand, as the study of brain connectivity gains increasing interest, network-variate modeling has emerged as an advanced analytical framework capable of accommodating the underlying dependence and brain topological architectures. In contrast to marginal and univariate analyses, network-variate modeling directly handles the (weighted) adjacency matrix of connectivity, enabling an explicit characterization of the biological structure. Depending on the objectives of the study, the network-variate can serve three distinct roles. Firstly, it can be employed solely to describe neurobiological profiles of the brain using different types of graphical modeling techniques in light of topological assumptions (Chen et al., 2023; Wang and Guo, 2020; Zhang et al., 2020). Secondly, when associated with a behavioral outcome, the network-variate can be treated as a predictor, involving specific matrix/tensor operations such as outer products (Wang et al., 2021) to transform the predictive component into a linear term (Zhao et al., 2022). Finally, to investigate the impact of covariates or exposures on the variation of connectivity, the network variate can be treated as an outcome in a network-response regression. In this case, the coefficient parameters reveal a matrix or tensor format and can be further decomposed to elucidate the latent effect

mechanisms (Zhang et al., 2023; Zhao et al., 2023; Kong et al., 2019; Hu et al., 2021). It is evident that the last category could shed light on genetic association analyses involving connectivity or network-variate phenotypes.

From a study design perspective, sample relatedness is highly prevalent and almost unavoidable in quantitative genetics studies. Such relatedness could be induced by recruitment from the same family or pedigree, or unknown or uncertain relationships including distant levels of unknown common ancestry (Eu-Ahsunthornwattana et al., 2014). Failure to account for potential sample structures within GWAS can lead to spurious results (Helgason et al., 2005), emphasizing the necessity for appropriate correction methods. One common approach to address sample structures is to include a random effect component to account for known or unknown relatedness. Building on linear mixed-effects models (LMMs), various numerical implementation approaches proposed in recent years to characterize genetic associations accommodating population substructure and potential sample relatedness (Kang et al., 2010; Zhou and Stephens, 2012). However, most of these approaches are designed for univariate phenotypes or vector-variate multivariate phenotypes, and there is currently no existing framework that adequately considers or readily applies to network-variate phenotypes.

To address the above limitations, we propose a **Bayesian Network-phenotype Mixed Effect** model (BNME) to perform genetic association analyses with brain connectivity phenotype. Within this unified modeling framework, we simultaneously characterize genetic contributions and identify affected phenotypic network components, while quantifying their uncertainty. To leverage the biological knowledge that brain connectivity operates via sub-

network configurations, our approach assumes that risk genetic variants influence network alternations by acting upon specific subnetwork/subnetwork units that are to be uncovered. By imposing shrinkage and sparsity priors on the effect parameters, we can map out the genetically targeted brain subnetworks that play a critical role to guide future intervention strategies. In contrast to recent works on network-response genetic association analyses including [Zhao et al. \(2023\)](#) and [Kong et al. \(2019\)](#), our proposed method incorporates pedigree information and accounts for sample structures, ensuring the reliability and validity of the findings. In our data application, we apply the BNME model to study the genetic bases of brain structural connectivity in the Human Connectome Project (HCP), accommodating its extensive family structures. Lastly, despite the proposed model being motivated by brain connectivity genetic studies, it can be readily extended to perform general network- or matrix-response mixed effects modeling. To the best of our knowledge, this work is among the very first to develop such a modeling framework, which directly fulfills an urgent need to capture multi-source of random variability for a growing collection of network data in biomedical studies.

The remainder of the article is organized as follows. In Section 2, we describe the proposed LMM with a network response (Section 2.1), the prior specifications (Section 2.2), the posterior inference procedure (Section 2.3), and the non-genetic effect adjustment (Section 2.4). We conduct simulation studies to evaluate the proposed model compared with existing alternatives in Section 3, followed by an application to HCP brain connectivity genetics data in Section 4. In the end, we conclude the paper with a discussion in Section 5.

2 Method

2.1 Linear mixed-effect model with a network phenotype

We first describe the problem setting in the context of GWAS with genetic correlation, though the model formulation represents a general network-response mixed-effect model that can be extended to other applications. Assume the study includes N subjects with known pedigree structure or unknown relationship. For subject i ($i = 1, \dots, N$), let z_i denote the genotype of interest which is encoded as 0, 1 or 2 according to the number of copies for the tested allele, $\mathbf{x}_i \in \mathbb{R}^{P \times 1}$ represents a set of covariates, and $\mathbf{A}_i \in \mathbb{R}^{V \times V}$ denotes the network phenotype summarized by a graphical matrix. With \mathbf{A}_i stacked across all the subjects, we have the network phenotype array $\mathcal{A} \in \mathbb{R}^{V \times V \times N}$. Specifically in the application of brain network studies, with images processed under a common brain atlas with V nodes, both structural and functional brain connectivity can be viewed as an indirect graph across vertex set $\{1, \dots, V\}$. Thus, \mathbf{A}_i becomes a symmetric matrix to summarize brain connectivity for each subject with diagonal elements to be zero, and its (k, l) th entry a_{ikl} , $0 < k \neq l \leq V$ represents the connection between nodes k and l characterizing either the white matter fiber tracts (structural connectivity) or statistical dependence of functional time course (functional connectivity). We adopt continuous metrics to measure structural and functional connections. After normalizing the genetic variant and each phenotypic connection, we propose the

following genetic association model for the indirect network response,

$$\mathbf{A}_i = \Theta z_i - \text{Hol}[\Theta z_i] + (\mathbf{B}_i - \mathbf{B}_i^T) + (\mathbf{E}_i - \mathbf{E}_i^T). \quad (1)$$

Here, $\Theta \in \mathbb{R}^{V \times V}$ is the symmetric coefficient matrix to capture the genetic effect on the network phenotype, $\text{Hol}[\cdot]$ is the operation to hollow out the diagonal elements to form a diagonal matrix, $\mathbf{B}_i \in \mathbb{R}^{V \times V}$ is the symmetric random polygenic effect matrix, and $\mathbf{E}_i \in \mathbb{R}^{V \times V}$ is the symmetric random error matrix characterizing the environmental effects. To demonstrate the main idea, we include only genetic fixed effect at this moment, and we will extend the model to include non-genetic covariates afterwards. Model (1) can be viewed as an extension of the traditional linear mixed effect model for genetic association with univariate or multivariate phenotypes accommodating sample relatedness. In addition to a matrix-variate phenotype, we design both mean and variance components to maintain their original functions while satisfying the symmetric and hollow structure of the indirect network as shown in the right-hand side of (1). Specifically, for the genetic and environmental effect matrix, by stacking each of them across all the subjects, we have the random effect tensor $\mathcal{B} \in \mathbb{R}^{N \times V \times V}$ and residual error tensor $\mathcal{E} \in \mathbb{R}^{N \times V \times V}$ with

$$\text{vec}(\mathcal{B}) \sim \text{N} \left\{ \begin{pmatrix} 0 \\ \vdots \\ 0 \end{pmatrix}, \text{Diag} \begin{pmatrix} \sigma_{11}^{(a)} \\ \vdots \\ \sigma_{VV}^{(a)} \end{pmatrix} \otimes \Lambda \right\}, \quad \text{vec}(\mathcal{E}) \sim \text{N} \left\{ \begin{pmatrix} 0 \\ \vdots \\ 0 \end{pmatrix}, \text{Diag} \begin{pmatrix} \sigma_{11}^{(e)}/2 \\ \vdots \\ \sigma_{VV}^{(e)}/2 \end{pmatrix} \otimes \mathbf{I}_N \right\},$$

where $\text{Diag}(\cdot)$ constructs the diagonal matrix formed by the inside vector, $\mathbf{I}_N \in \mathbb{R}^{N \times N}$ is the identify matrix, and $\Lambda \in \mathbb{R}^{N \times N}$ is the kinship matrix estimated by pedigree information for known family structures or genotypic relationship for unknown relatedness (Eusunthornwattana et al., 2014). By proposing so, we can show the phenotypic variance of each connection $\text{Var}(\mathbf{a}_{kl}) = 2\sigma_{kl}^{(a)}\Lambda + \sigma_{kl}^{(e)}\mathbf{I}_N$, $\mathbf{a}_{kl} = (a_{1kl}, \dots, a_{Nkl})^T, k \neq l$, consistent with the existing literature (Kang et al., 2010).

Given the size of commonly used brain atlas can be large with V in the range of 200 to 1000, directly performing estimation on model (1) is not ideal under a high-dimensional parameter space. More importantly, considering the primary interest to investigate the genetic association with brain network architectures, the topological structure can not be plausibly reflected by ignoring the dependence within the genetic coefficient matrix. To address so, we adopt the following Tucker decomposing under a symmetry constrain for the coefficient matrix

$$\Theta = \sum_{h=1}^H \eta_h \boldsymbol{\theta}_h \circ \boldsymbol{\theta}_h, \quad (2)$$

where \circ represents the outer product, and $\boldsymbol{\theta}_h = (\theta_{h1}, \dots, \theta_{hV})^T, h = 1, \dots, H$ are column coefficient vectors. From a neurobiological perspective, each $\boldsymbol{\theta}_h \circ \boldsymbol{\theta}_h$ describes an effect network component adjusted by a weight parameter η_h . Combining models (1) and (2), we allow the genetic variant delivers its impact on the phenotype via a series of signaling network architectures.

2.2 Prior specifications

We consider a fully Bayesian paradigm to estimate and perform inference for the proposed network-response LMM. For the fixed genetic effect component, we anticipate the genetic impact is sparse across the brain as shown by the existing empirical studies (Zhao et al., 2021a). Therefore, we assign the following combination of point mass mixture prior and shrinkage prior

$$\eta_h \sim (1 - \tau_h)\delta_0 + \tau_h\mathcal{N}(0, \omega); \quad \theta_{hv} \sim \mathcal{L}(\nu), \quad h = 1, \dots, H; v = 1, \dots, V. \quad (3)$$

Here, τ_h is the latent selection indicator to determine whether a network component is significantly impacted by the genotype as a whole. When $\tau_h = 1$, the weight parameter η_h is generated from a noninformative Normal prior with a large variance parameter ω ; otherwise, we assign η_h to a point mass at zero denoted by δ_0 to remove the whole component from the model. In real practice, with the number of effect component H unknown, such a specification of sparsity could efficiently assist the determination of the number of associated phenotypic network configurations during the learning process. As shown in our numerical studies, by imposing a conservative value to H , our model can correctly uncover the signaling network phenotypes. To specify priors for latent indicators τ_h , one can either impose a non-informative Bernoulli distribution for each of the elements, or resort to a more informative prior by incorporating additional biological structure (Li and Zhang, 2010). For

the coefficients, we assign a Laplace prior $\mathcal{L}(\nu)$ with a scale parameter ν to shrink the noise effect to a close to zero value. To further facilitate a straightforward posterior computation, following [Park and Casella \(2008\)](#), we represent each Laplace prior by a scale mixture of normals for each $h = 1, \dots, H$,

$$\boldsymbol{\theta}_h \sim N(\mathbf{0}, \mathcal{D}_h); \quad \mathcal{D}_h = \text{Diag}(\sigma_{h1}, \dots, \sigma_{hV}); \quad \sigma_{hv} \sim \frac{\nu^2}{2} \exp\left(-\frac{\nu^2 \sigma_{hv}}{2}\right) d\sigma_{hv}, v = 1, \dots, V. \quad (4)$$

Combining priors (3) and (4), we characterize the phenotypic signals in a hierarchical way with a group-level sparsity to induce the selection of a phenotypic network as a whole and a within-group shrinkage to identify the actual signaling subnetwork structure within selected ones. In contrast to existing sparse group selection or shrinkage models that primarily focus on group structural covariates ([Simon et al., 2013](#); [Chang et al., 2018](#)), our research emphasizes the network-variate outcome, which captures the associations between covariates and latent topological hierarchies. Additionally, we opt for shrinkage priors for individual coefficients instead of point mass mixture priors, driven by computational considerations that result in lower computational costs for shrinkage priors. However, it is important to note that the Laplace prior can be readily replaced with spike-and-slab types of priors or other graphical priors ([Chang et al., 2018](#); [Stingo et al., 2011](#)) to impose sharp sparsity or incorporate spatial information. Finally, we assign non-informative inverse gamma (IG) prior for variances $\sigma_{kl}^{(a)}, \sigma_{kl}^{(e)}$ with shape and scale parameters α and β , respectively, and a relatively large value for the rest of the variance parameters during implementation. For the tuning

parameters including the number of informative subnetworks H and scale parameter ν , we consider a grid search of them and choose the optimal values using the Bayesian information criterion (BIC). Our numerical experience suggests that this strategy is effective in practical applications.

2.3 Posterior likelihood and inference for BNME

To perform posterior inference for the proposed BNME model, we first develop the posterior likelihood for the collect of unknown parameters denoted as $\zeta = \left[\left\{ \boldsymbol{\theta}_h, \eta_h, \tau_h, (\sigma_{hv})_{v=1}^V \right\}_{h=1}^H, (\sigma_{vv'}^{(a)})_{v,v'=1}^V, (\sigma_{vv'}^{(e)})_{v,v'=1}^V, \nu \right]$. Based on the observed data $\mathcal{O} = (\mathbf{A}_i, z_i, \Lambda; i = 1, \dots, N)$, the joint posterior distribution follows

$$\begin{aligned} \pi(\zeta | \mathcal{O}) &\propto \prod_i \pi(\mathbf{A}_i, z_i, \Lambda | \{\boldsymbol{\theta}_h, \eta_h, \tau_h\}_{h=1}^H, (\sigma_{vv'}^{(a)})_{v,v'=1}^V, (\sigma_{vv'}^{(e)})_{v,v'=1}^V) \\ &\quad \times \prod_v \left\{ \prod_h \pi(\boldsymbol{\theta}_{hv} | \sigma_{hv}, \nu) \pi(\sigma_{hv}) \prod_{v'} \pi(\sigma_{vv'}^{(a)}) \pi(\sigma_{vv'}^{(e)}) \right\} \prod_h \left\{ \pi(\tau_h) \pi(\eta_h | \tau_h) \right\}, \end{aligned} \quad (5)$$

which combines the conditional observed data likelihood with prior distributions. Given uncertainty quantification is an essential component for genetic association analyses, instead of pursuing point estimates via optimization algorithms, we develop a Markov chain Monte Carlo (MCMC) sampling algorithm for posterior inference based on a combination of Gibbs samplers and Metropolis-Hastings (MH) updates. Under random initializations, we cycle through the following steps:

- For $h = 1 \dots H$, $k = 1 \dots V$, $l = 1 \dots V$, denote the (k, l) th entry of matrix $\{\mathbf{A}_i -$

$\sum_{h' \neq h} \eta_{h'} \boldsymbol{\theta}_{h'} \circ \boldsymbol{\theta}_{h'} z_i$ as \tilde{a}_{iklh} , and define $\tilde{\mathbf{a}}_{klh} = (\tilde{a}_{1klh}, \dots, \tilde{a}_{Nklh})^T$, $\mathbf{z} = (z_1, \dots, z_N)^T$.

Sample θ_{hk} from $N(\mu_{\theta_{hk}}, \sigma_{\theta_{hk}})$ with $\sigma_{\theta_{hk}} = \left(\sum_{l \neq k} \eta_h^2 \theta_{hl}^2 \mathbf{z}^T \left(\sigma_{kl}^{(a)} \Lambda + \sigma_{kl}^{(e)} I \right)^{-1} \mathbf{z} + \sigma_{hk}^{-1} \right)^{-1}$

and $\mu_{\theta_{hk}} = \sum_{l \neq k} \tilde{\mathbf{a}}_{klh}^T \left(\sigma_{kl}^{(a)} \Lambda + \sigma_{kl}^{(e)} I \right)^{-1} \mathbf{z} \eta_h \theta_{hl} \sigma_{\theta_{hk}}$

- For $h = 1 \dots H$, $k = 1 \dots V$, sample σ_{hk}^{-1} from an Inverse Normal distribution $\text{IN}(\frac{\nu}{\theta_{hk}}, \nu^2)$.
- For $h = 1 \dots H$, when $\tau_h = 0$, set η_h to be zero. Otherwise, denote the (k, l) th entry of matrix $\boldsymbol{\theta}_h \circ \boldsymbol{\theta}_h z_i$ as q_{iklh} , and $\mathbf{q}_{klh} = (q_{1klh}, \dots, q_{Nklh})^T$. Update between subnetwork coefficient η_h from their corresponding posterior Normal distribution $N(\mu_{\eta_h}, \sigma_{\eta_h})$ with $\sigma_{\eta_h} = \left(\sum_{k < l} \mathbf{q}_{klh}^T (\sigma_{kl}^{(a)} \Lambda + \sigma_{kl}^{(e)} I)^{-1} \mathbf{q}_{klh} + \omega^{-1} \right)^{-1}$, and $\mu_{\eta_h} = \sum_{k < l} \tilde{\mathbf{a}}_{klh}^T (\sigma_{kl}^{(a)} \Lambda + \sigma_{kl}^{(e)} I)^{-1} \mathbf{q}_{klh} \Sigma_{\eta_h}$.
- For $h = 1 \dots H$, define $l_0 := \frac{C}{\omega} \exp(-\frac{1}{2}(\frac{C\eta_h}{\omega})^2)$ and $l_1 := \frac{1}{\omega} \exp(-\frac{1}{2}(\frac{\eta_h}{\omega})^2)$ with C a large constant. We then update the selection indicators τ_h following the posterior Bernoulli distributions $\text{Bern}(\frac{l_1}{l_0 + l_1})$.
- For $v = 1 \dots V$, $v' = 1 \dots V$, update $\sigma_{vv'}^{(a)}$ by sampling a proposed value $\sigma_{vv'}^{(a)p}$ from a random walk proposal distribution $N(\sigma_{vv'}^{(a)}, \rho_1^2)$, and setting $\sigma_{vv'}^{(a)} = \sigma_{vv'}^{(a)p}$ with probability $\min\{1, R_1\} I\{\sigma_{vv'}^{(a)p} > 0\}$, where $R_1 = \frac{\pi(\sigma_{vv'}^{(a)p} | \mathcal{O}, \{\eta_h, \tau_h, \boldsymbol{\theta}_h\}_{h=1}^H, \sigma_{k \neq v, l \neq v'}^{(a)}, \sigma^{(e)})}{\pi(\sigma_{vv'}^{(a)} | \mathcal{O}, \{\eta_h, \tau_h, \boldsymbol{\theta}_h\}_{h=1}^H, \sigma_{k \neq v, l \neq v'}^{(a)}, \sigma^{(e)})}$, with $\pi(\sigma_{vv'}^{(a)} | \mathcal{O}, \{\eta_h, \tau_h, \boldsymbol{\theta}_h\}_{h=1}^H, \sigma_{k \neq v, l \neq v'}^{(a)}, \sigma^{(e)}) \propto \mathcal{L}(\mathcal{O} | \boldsymbol{\zeta}) \{\sigma_{vv'}^{(a)}\}^{-\alpha-1} \exp(-\frac{\beta}{\sigma_{vv'}^{(a)}})$ the full conditional.
- For $v = 1 \dots V$, $v' = 1 \dots V$, update $\sigma_{vv'}^{(e)}$ by sampling a proposed value $\sigma_{vv'}^{(e)p}$ from a random walk proposal distribution $N(\sigma_{vv'}^{(e)}, \rho_2^2)$ and setting $\sigma_{vv'}^{(e)} = \sigma_{vv'}^{(e)p}$ with probability $\min\{1, R_2\} I\{\sigma_{vv'}^{(e)p} > 0\}$, where $R_2 = \frac{\pi(\sigma_{vv'}^{(e)p} | \mathcal{O}, \{\eta_h, \tau_h, \boldsymbol{\theta}_h\}_{h=1}^H, \sigma^{(a)}, \sigma_{k \neq v, l \neq v'}^{(e)})}{\pi(\sigma_{vv'}^{(e)} | \mathcal{O}, \{\eta_h, \tau_h, \boldsymbol{\theta}_h\}_{h=1}^H, \sigma^{(a)}, \sigma_{k \neq v, l \neq v'}^{(e)})}$, with $\pi(\sigma_{vv'}^{(e)} | \mathcal{O}, \{\eta_h, \tau_h, \boldsymbol{\theta}_h\}_{h=1}^H, \sigma^{(a)}, \sigma_{k \neq v, l \neq v'}^{(e)})$

$$\mathcal{O}, \{\eta_h, \tau_h, \boldsymbol{\theta}_h\}_{h=1}^H, \sigma^{(a)}, \sigma_{k \neq v, l \neq v'}^{(e)} \propto \mathcal{L}(\mathcal{O} \mid \boldsymbol{\zeta}) \{\sigma_{vv'}^{(e)}\}^{-\alpha-1} \exp\left(-\frac{\beta}{\sigma_{vv'}^{(e)}}\right) \text{ the full conditional.}$$

Based on the posterior samples, the convergence of the algorithm is examined by trace plots and GR method (Gelman et al., 1992). To characterize the genetic impact and dissect the associated signaling brain network configurations, we first determined the overall phenotypic subnetworks linked with the genetic variant based on a 0.5 cutoff of the posterior mean for each τ_h . This cutoff is adopted in light of the median probability model (Hastie et al., 2004). Under a conservative H , most of the risk genetic variants are associated with less than H brain connectivity subnetworks. When none of the elements in $\{\tau_h\}_{h=1}^H$ surpasses the cutoff, the genetic variant does not provide a significant impact on any component of the network phenotype. For the selected subnetworks with τ_h larger than the cutoff, the genetic effect over network structures is captured by the posterior mean of θ_h . Despite that a Laplace prior does not impose strict sparsity, we can determine the specific brain network configurations that are most relevant to the genetic impact by extracting the elements from θ_h with a credible interval excluding zero. Eventually, our model could provide estimation and inference for the risk genetic factors and their most influencing phenotypic topological elements.

2.4 Covariates adjustment

In genetic association studies, it is a standard practice to adjust for non-genetic covariates, such as demographics and genetic principle components. In this paper, extending an existing

projection approach for multivariate outcomes (Ge et al., 2016; Zhao et al., 2022), we account for the effect of covariates in addition to model (1). Denote covariate matrix as $\mathbf{X} = (\mathbf{x}_1, \dots, \mathbf{x}_N)^T \in \mathbb{R}^{N \times P}$, and we define a projection matrix $\mathbf{W} = \mathbf{I}_{N \times N} - \mathbf{X}(\mathbf{X}^T \mathbf{X})^{-1} \mathbf{X}^T$. Clearly, \mathbf{W} is symmetric and idempotent matrix with a rank of $(N - P)$, and this further indicates that \mathbf{W} can be decomposed as $\mathbf{W} = \mathbf{U}^T \mathbf{U}$, where matrix $\mathbf{U} \in \mathbb{R}^{(N-P) \times N}$ and satisfies $\mathbf{U} \mathbf{U}^T = \mathbf{I}_{N-P}$ and $\mathbf{U} \mathbf{X} = \mathbf{0}$. Through matrix \mathbf{U} , the data can be projected from the N dimensional space onto an $(N - P)$ dimensional subspace. This facilitates an efficient way to remove the nuisance covariate effects by projecting both sides in the original model via

$$\mathbf{U} \mathbf{A} = \Theta \mathbf{U} z + \mathbf{U} \mathbf{B} + \mathbf{U} \mathcal{E}. \quad (6)$$

Model (6) indicates that by replacing the connectivity array \mathbf{A} with $\tilde{\mathbf{A}} = \mathbf{U} \mathbf{A}$, genotype z with $\tilde{z} = \mathbf{U} z$ and the kinship matrix Λ with $\tilde{\Lambda} = \mathbf{U} \Lambda \mathbf{U}^T$, the joint posterior distribution will follow the same structure as (5). Hence, all sampling procedures can be adopted accordingly.

3 Simulation Studies

We carry out simulation studies to evaluate the proposed BNME to uncover genetic signals and the associated phenotypic network configurations under related samples. To mimic the data dimension in our data application, we assign sample sizes $N = 100$ and 500 with brain

connectivity generated under a brain atlas with $V = 50$. We consider two scenarios on the phenotypic network configurations that are highly impacted by the genetic factor. In the first scenario, we generate a single phenotypic subnetwork that is linked with the genetic variant, and we set $\eta_1 = 1$. In the second scenario, we create a more challenging setting by generating three subnetworks with the associated weight parameter η_h equals 0.7, 0.3 and 0, respectively. The third subnetwork is not linked to the genetic variant, allowing us to evaluate the performance of our model in detecting the true number of signaling phenotypic components. For both scenarios, we consider a range of sparsity levels for each θ_h by imposing 50%, 90% and 100% of the elements within the vector to be zero to define the genetically associated clique subnetworks. As shown in Figure 1, we provide the signal patterns upon the whole network phenotype under 50% and 90% sparsity levels for the second scenario assembled across subnetworks. Of note, when sparsity level is 100%, the genotype does not impact any of the phenotypic structures, facilitating a test on a noise genetic variant. For the variance components, we first generate a kinship matrix Λ with diagonal entries to be 1 and off-diagonal entries ranging from (0,1) to be consistent with real practice. Then we set each of the polygenic effect variance $\sigma_{vv'}^{(a)}$ to be 1.5 and the environmental effect variance $\sigma_{vv'}^{(e)}$ to be 1. Finally, for the fix effects, we sample the genotype for each subject from $\{0, 1, 2\}$, and add three different types of non-genetic covariates including one generated from a Bernoulli distribution $\text{Bern}(0.5)$, one from a Uniform distribution $\mathcal{U}(-0.5, 0.5)$, and one from a Normal distribution $\mathcal{N}(-0.5, 0.5)$. Each of the fixed effect coefficients are generated from $\mathcal{N}(0.3, 0.5)$ and fixed for all the settings. Overall, we consider 12 settings with different sample sizes and

phenotypic signal patterns, and we generated 200 Monte Carlo datasets for each setting.

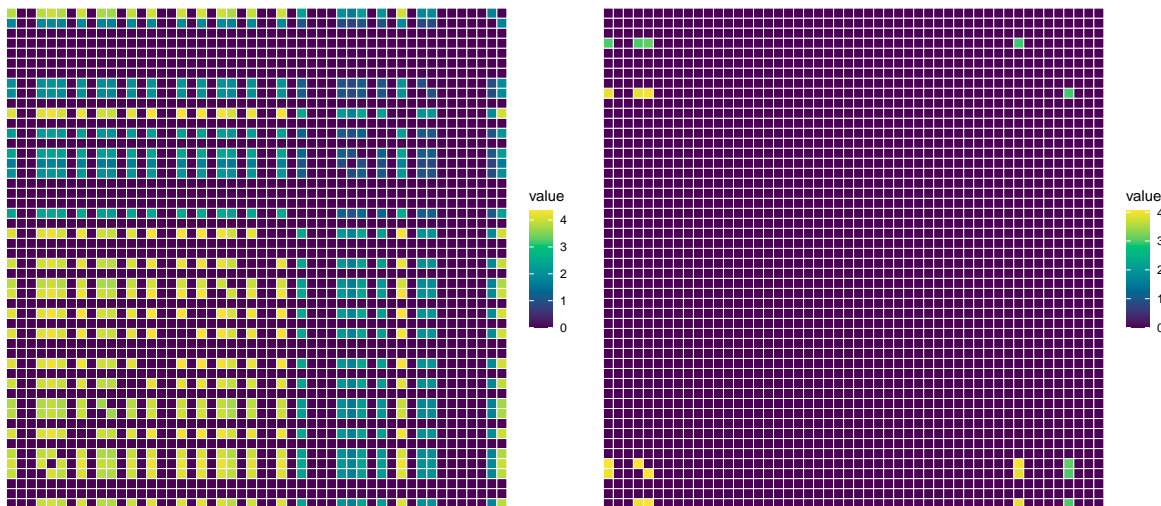


Figure 1: Assembled signal patterns upon the whole phenotypic network at the sparsity levels of 50% (left panel) and 90% (right panel) under the second scenario with three subnetworks.

To implement the proposed BNME model, we set $\alpha = \beta = 0.01$ for a noninformative support of IG priors. To assess the robustness of the model, we directly set $H = 3$ which is larger than the actual number of the associated phenotypic subnetworks for both scenarios, and we determine ν by a grid search from $(0.5, 0.8, 1)$ based on BIC. The MCMC algorithm is performed for 5,000 iterations after 2,000 burn-in, and both trace plots and GR value indicate a convergence. For the competing methods, given there is no existing regression approach that can accommodate a network outcome with mixed effects, we extract unique edges from the phenotype matrix. With each of the upper diagonal elements of A_i as a phenotypic trait, we implement a linear mixed-effect model (LMM) using the `lme4` package in R, linear mixed-effects kinship model (LMEKIN) using the `coxme` package in R and one of

the most popular GWAS pipelines for related samples and univariate phenotype Genome-wide Efficient Mixed Model Association (GEMMA, [Zhou and Stephens, 2012](#)). To evaluate both estimation and feature selection, we consider the following performance metrics: (a) root mean predicted square error (RMSE) of \mathbf{A}_i , (b) sensitivity (Sen_e) and specificity (Spe_e) for distinguishing signaling phenotypic elements captured by the nonzero elements in Θ , and (c) specificity (Spe_g) for identifying noise genetic variant when sparsity level is 100%. All the simulation results are summarized in Table 1.

Based on the results, we conclude that our proposed BNME model demonstrates excellent performance in uncovering genetic effects, identifying associated phenotypic network configurations, and distinguishing noise genetic variants. Specifically, the BNME exhibits a significantly smaller RMSE compared to alternative methods indicating higher estimation accuracy. Our method also achieves over 90% phenotypic sensitivity and specificity across all the simulation settings, and genotypic specificity when the sparsity level is 100%, indicating its ability to uncover the associated phenotypic networks for the risk genotype and distinguish the noise genetic variant. When comparing different settings, we consistently observe improvements in performance metrics for all methods as the sample size increases. As anticipated, a higher sparsity level aids in signal identification for all the methods. Notably, when sparsity reaches 100% with no associated phenotypic connections, given that our method allows to exclude the noise phenotypic component entirely, it successfully detects this situation as evidenced by a close to one Sen_g . Moreover, as more phenotypic subnetworks are impacted, including a noise subnetwork, we observe a notable decrease in the accuracy

of phenotypic feature selection for all competing methods. However, our method maintains its superior performance, indicating its robustness and ability to uncover the true signaling phenotypic subnetworks even under a misspecified subnetwork number H . Finally, in the comparison among competing methods, both LMEKIN and GEMMA demonstrate similar performance, surpassing the traditional LMM. Their performance in the presence of a noise genotype suggests a high risk of false positives when considering GWAS under a network phenotype.

4 Real data application

4.1 Imaging genetics data for HCP

We implement our model to the imaging genetics data from the Human Connectome Project (HCP). HCP is a landmark study of healthy subjects that has collected a rich set of imaging, behavioral and genetic data. In the current analyses, we adopt the WU-Minn HCP minimally processed S1200 release that includes over 1,000 healthy young adults aged 22 to 37 years. For each subject, both T1 magnetic resonance imaging (MRI) and diffusion MRI (dMRI) are available, allowing the construction of brain structural connectivity to capture the white matter fiber tracts connecting different brain regions. Specifically, based on the minimally preprocessed dMRI and T1 data from ConnectomeDB, we first generate the whole-brain tractography for each subject via a recent probabilistic tractography pipeline ([Zhang et al.](#),

Table 1: Simulation results for all the methods under different settings range from sample sizes (N), sparsity levels and phenotypic subnetworks ($\#$ Sub). The results are summarized over 200 MC datasets and the standard deviations are included in the parenthesis.

# Sub	Sparsity	Model	N=100				N=500			
			RMSE	Spe _e	Sen _e	Spe _g	RMSE	Spe _e	Sen _e	Spe _g
1	50%	BNME	0.13 (0.05)	0.96 (0.04)	1.00 (0.00)	-	0.04 (0.02)	0.97 (0.03)	1.00 (0.00)	-
		LMM	0.71 (0.22)	0.94 (0.12)	0.86 (0.10)	-	0.32 (0.06)	0.95 (0.05)	0.98 (0.01)	-
		LMEKIN	0.25 (0.10)	0.94 (0.14)	0.93 (0.05)	-	0.24 (0.07)	0.95 (0.05)	0.98 (0.03)	-
		GEMMA	0.25 (0.13)	0.94 (0.14)	0.93 (0.03)	-	0.20 (0.04)	0.95 (0.05)	0.99 (0.00)	-
	90%	BNME	0.53 (0.14)	0.99 (0.01)	1.00 (0.00)	-	0.34 (0.30)	0.99 (0.01)	1.00 (0.00)	-
		LMM	0.58 (0.02)	0.94 (0.01)	0.99 (0.02)	-	0.35 (0.26)	0.95 (0.04)	1.00 (0.00)	-
		LMEKIN	0.26 (0.07)	0.93 (0.03)	0.99 (0.01)	-	0.28 (0.06)	0.95 (0.05)	0.99 (0.00)	-
		GEMMA	0.23 (0.09)	0.95 (0.06)	0.99 (0.01)	-	0.22 (0.03)	0.95 (0.02)	0.99 (0.00)	-
	100%	BNME	0.01 (0.02)	1.00 (0.01)	-	0.96	0.01 (0.01)	1.00 (0.00)	-	1.00
		LMM	0.58 (0.02)	0.95 (0.01)	-	0.00	0.25 (0.01)	0.95 (0.01)	-	0.00
		LMEKIN	0.22 (0.02)	0.95 (0.02)	-	0.00	0.25 (0.01)	0.95 (0.01)	-	0.02
		GEMMA	0.22 (0.02)	0.95 (0.01)	-	0.00	0.25 (0.01)	0.94 (0.01)	-	0.00
3	50%	BNME	0.14 (0.03)	0.90 (0.04)	0.92 (0.08)	-	0.09 (0.03)	0.93 (0.05)	0.88 (0.08)	-
		LMM	0.71 (0.23)	0.90 (0.12)	0.62 (0.12)	-	0.32 (0.06)	0.95 (0.05)	0.87 (0.06)	-
		LMEKIN	0.39 (0.11)	0.93 (0.14)	0.70 (0.18)	-	0.23 (0.06)	0.93 (0.04)	0.90 (0.03)	-
		GEMMA	0.39 (0.09)	0.94 (0.03)	0.69 (0.19)	-	0.23 (0.06)	0.95 (0.05)	0.94 (0.04)	-
	90%	BNME	0.21 (0.06)	0.99 (0.01)	0.95 (0.09)	-	0.12 (0.20)	0.99 (0.02)	1.00 (0.00)	-
		LMM	0.71 (0.23)	0.94 (0.12)	0.73 (0.13)	-	0.25 (0.01)	0.95 (0.01)	0.97 (0.03)	-
		LMEKIN	0.23 (0.10)	0.95 (0.09)	0.85 (0.09)	-	0.21 (0.05)	0.96 (0.02)	0.95 (0.05)	-
		GEMMA	0.21 (0.06)	0.96 (0.07)	0.85 (0.09)	-	0.21 (0.05)	0.95 (0.01)	0.99 (0.01)	-
	100%	BNME	0.01 (0.01)	1.00 (0.00)	-	1.00	0.02 (0.04)	1.00 (0.02)	-	0.90
		LMM	0.58 (0.02)	0.94 (0.01)	-	0.00	0.25 (0.01)	0.94 (0.01)	-	0.00
		LMEKIN	0.22 (0.09)	0.95 (0.03)	-	0.00	0.21 (0.15)	0.95 (0.04)	-	0.03
		GEMMA	0.23 (0.13)	0.95 (0.01)	-	0.01	0.24 (0.01)	0.94 (0.01)	-	0.01

*Phenotypic sensitivity does not exist at a 100% sparse level with no connection associated with the genotype.

2018). We then perform the anatomical parcellation via Desikan-Killiany (DK) atlas (Desikan et al., 2006) including 68 cortical surface regions and 19 subcortical regions. To extract the streamlines linking each pair of ROIs, a series of steps including dilation of each gray matter ROI to incorporate white matter regions, separation of the streamlines connecting

several ROIs into parts, and removing obvious outlier streamlines are conducted. Subsequently, the mean fractional anisotropy (FA) value along streamlines is used to evaluate the strength of structural connections. Eventually, we construct brain structural connectivity for 1,065 subjects. Comprehensive details are available elsewhere on HCP neuroimaging protocols ([Van Essen et al., 2013](#)) and our tractography pipeline ([Zhao et al., 2023](#)).

The young adult participants in HCP were also genotyped by Illumina’s MultiEthnic Global Array (MEGA) Chip and three specialized neuroimaging chips: Psych, NeuroX, and Immunochip. After standard data quality by excluding subjects with more than 10% missing SNPs or sex check failure, 1,010 subjects with both genotypes and phenotypes are included in our analyses. For the genetic variants, to mitigate computational cost, we focus on the 1,860 SNPs that were identified in the previous study to highly associate with brain structural network ([Zhao et al., 2023](#)). However, unlike the previous analyses that didn’t accommodate the sample relatedness, we consider family structure after creating the kinship matrix for 149 pairs of genetically-confirmed monozygotic twins (298 participants), 94 pairs of genetically-confirmed dizygotic twins (188 participants) and their non-twin siblings (524 participants). Besides the proposed BNME, we also implement GEMMA to conduct the genetic association analyses under our related samples. All the model implementations closely follow the simulation studies, and we account for age, gender, and the top ten genetic principal components in analyses.

4.2 Analysis results

Our goal is to identify risk genetic markers and their associated brain connectivity phenotypic components. Based on the posterior samples of η , we identify nine risk SNPs as shown in Table 2. After mapping those SNPs to the genes they belong to, we identify five unique gene variants including THSD7B, LINC01503, LOC105373693, CDH13 and SLC38A8. Among them, THSD7B and CDH13 have been considered to play an essential role in the development of the central nervous system and neural connectivity (Li et al., 2022; Wang et al., 2011; Polanco et al., 2021). Particularly, THSD7B has also been shown to associate with intellectual disability (Lyons-Warren et al., 2022); and CDH13 is related to various psychiatric disorders including ADHD and substance abuse (Rivero et al., 2013; Treutlein and Rietschel, 2011). To evaluate the neurogenetic processes of the selected genetic variants, we further perform a brain tissue-specific expression quantitative trait loci (eQTL) analysis via the UK Brain Expression Consortium (UKBEC, Ramasamy et al., 2014a). The consortium generated genotype and exon-specific expression data for 134 neuropathologically healthy subjects under ten different brain tissues, which allows us to evaluate each identified genetic variant on its alteration of tissue-specific and cross-tissue gene expressions within 100kb of the SNP (Zhao et al., 2023). Table 2 Column 3 shows the cross-tissue cis-effect p-value calculated in their BRAINEAC web server, and the regulated genes for each risk SNP. The small p-values of cross-tissue eQTLs reflect the molecular regulation through gene expression over different brain areas, consistent with the genetic association with brain network phenotypes.

Table 2: Significant genetic variants and their associated phenotypic structural subnetworks, along with cis-eQTL results obtained from UKBEC brain database.

SNP	eQTL			Phenotypic subnetworks	
	Chromosome	p-value	Regulated genes	# Association	Macroscale systems
rs2465095	2	9.30E-03	THSD7B	91	Subcortical, Parietal lobe
rs1918367	2	3.50E-02	GALNT13	91	Subcortical, Parietal lobe
rs4725467	7	2.20E-02	GALNTL5	325	Subcortical, Temporal lobe
rs10760611	9	5.00E-03	ASB6	20	Subcortical
rs4948428	10	2.50E-02	TMEM26	6	Subcortical
rs1537969	13	5.50E-02	SGCG	22	Subcortical, Temporal lobe
rs9928439	16	2.50E-02	SLC38A8	91	Subcortical, Temporal lobe
rs6563992	16	1.30E-03	ATP2C2	15	Subcortical
rs58090793	16	3.30E-03	ZDHHC7	3	Frontal lobe

We further investigate the associated brain subnetwork phenotypic components for each of the identified genetic signals. Visualization of each genetically associated brain network component is displayed in Figure 2, where the color of connections indicates the effect size of genetic association. Additionally, we summarized the macroscale structures involved in subnetworks for each identified SNP in Table 2. Our analysis revealed that cross-hemispheric connections and inter-subcortical connections accounted for the largest proportion of all the signaling connections. This finding aligns closely with previous literature, which has consistently demonstrated that genetic effects lead to alterations in white matter fiber tracts across brain hemispheres and subcortical structures (Jahanshad et al., 2013; Zhong et al., 2021; Zhao et al., 2021a). For instance, Zhong et al. (2021) investigated interhemispheric connectivity and highlighted the influence of genetic factors on the integrity and organization of connections between the two hemispheres. Similarly, Hibar et al. (2015) explored the

impact of common genetic variations on the subcortical brain and emphasized the role of genetics in shaping the variations of subcortical structures.

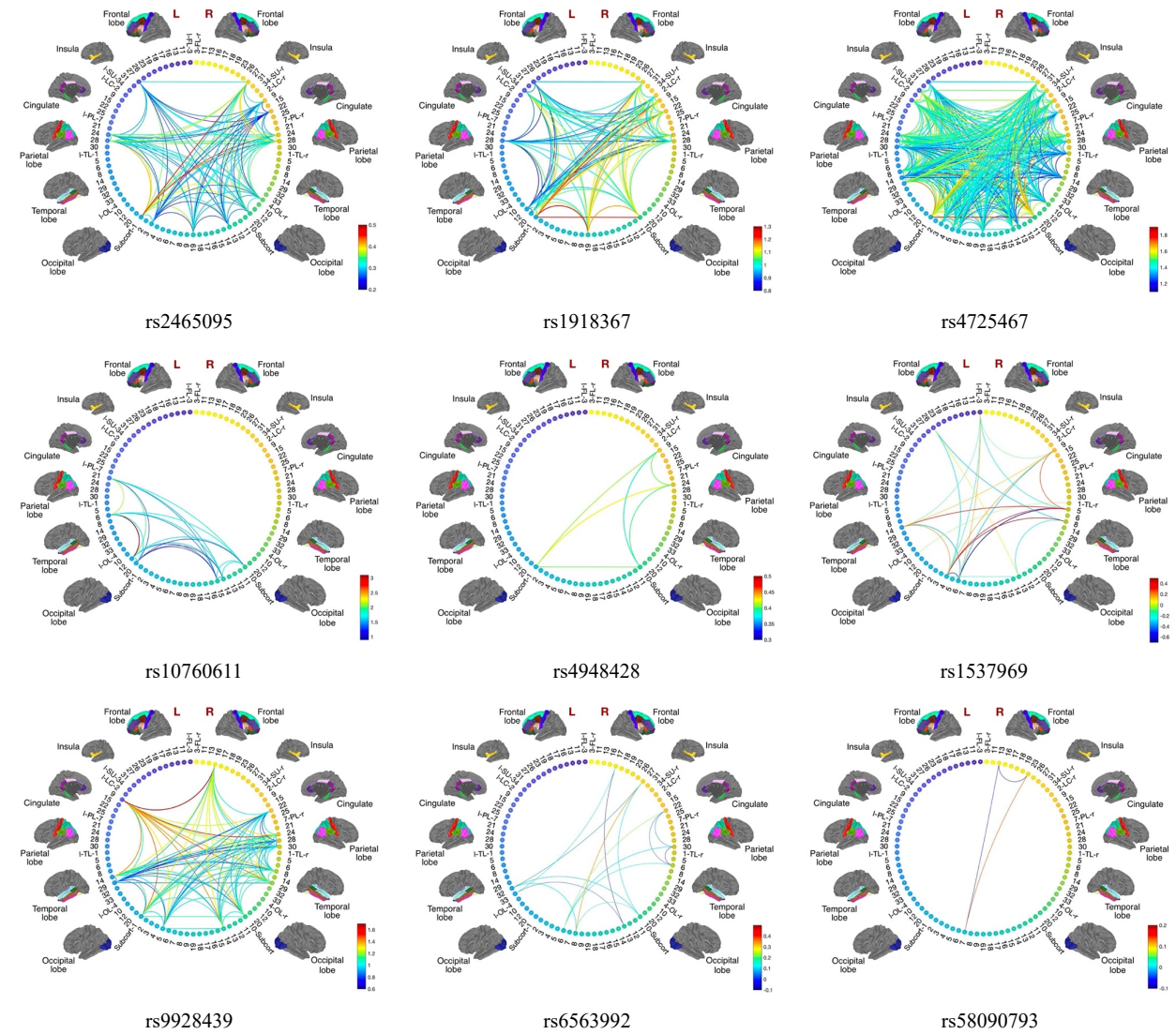


Figure 2: Nine SNPs and their associated brain network.

Finally, we conduct a comparison of imaging genetics results between our BNME model and GEMMA. GEMMA identifies a total of 35 SNPs that exhibit significant associations

with at least one brain connection. To assess the agreement in the top selected genetic variants between the two approaches, we map the top 35 selected SNPs from each method to their associated cytogenetic bands (Clark and Pazdernik, 2016) and examine the overlap in signals. Eventually, there are ten cytogenetic bands that encompass the genetic signals identified by both BNME and GEMMA. This indicates a certain degree of consistency in the genetic signals identified by the two methods, which lends support to the plausibility and reliability of our results. The detailed results are provided in the supplementary materials. Furthermore, we also visualize the number of associated brain connections for the top selected SNPs under each method in Figure 3. It is evident that, in contrast to BNME, which provides phenotypic subnetwork architecture specific to each genetic variant, the phenotypic signals identified under GEMMA appear to be extremely sparse and scattered. This result indicates that the majority of the SNPs identified under GEMMA are associated with a single brain connection, raising questions regarding the biological interpretability and meaningfulness of the observed genetic associations.

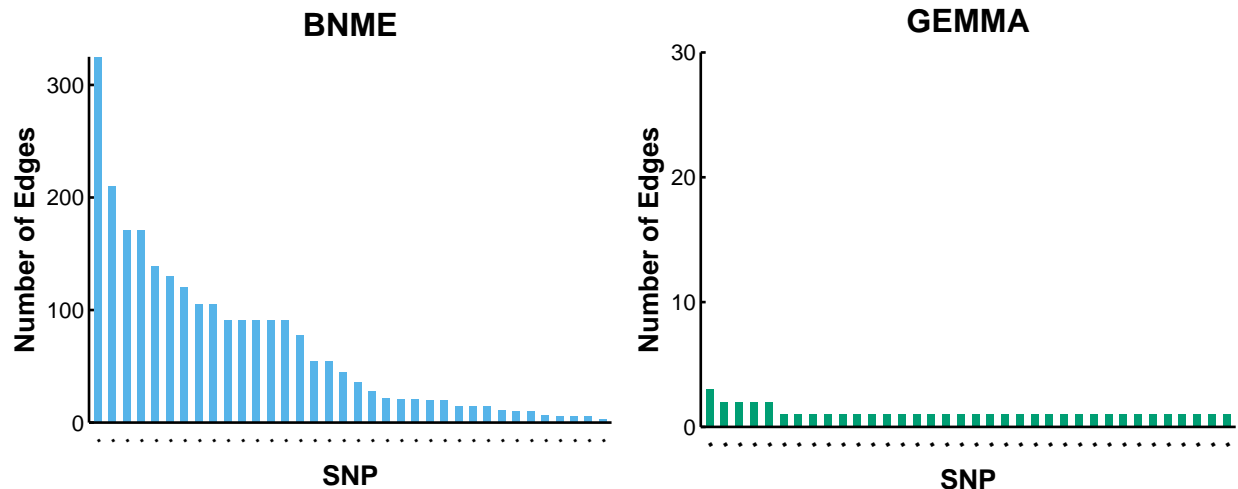


Figure 3: The number of significant edges within the phenotypic network identified by BNME and GEMMA

5 Discussion

In this paper, we present an innovative Bayesian network-response mixed effect model that addresses the challenges of genetic association studies in brain connectivity. Our model is specifically designed to capture the genetic contributions to phenotypic network configurations while accounting for family structures and unknown sample relatedness. To accommodate the biological architecture in the network phenotype, we consider the genetic variant influences the phenotype via a set of unknown subnetworks, where the targeted phenotypic subnetworks are uncovered through a hierarchical selection procedure. Through posterior inference, we effectively quantify the uncertainty associated with determining a risk genetic

variant and its impact on phenotypic network configurations. Extensive simulations demonstrate the superiority of our method over existing alternatives in estimating genetic effects and identifying relevant phenotypic elements with signaling capabilities. By applying the proposed method to the HCP cohort with excessive family structures, we obtain biologically interpretable results that shed light on uncovering the genetic underpinnings of brain structural connectivity.

In addition to its applicability to brain connectivity genetics studies, the proposed BNME model provides a fundamental framework for mixed-effect models involving network- or matrix-variate outcomes. As data collection in epidemiology and social studies becomes more complex, there is a growing need to analyze network-related or matrix-structured outcomes arising from related samples caused by pedigree or repeated measurements. By extending the random effect tensor, \mathcal{B} , to include an additional dimension corresponding to random slopes, along with the associated variance-covariance component, we can effectively capture more intricate sources of variation and address diverse modeling requirements.

Our current model formulation employs a decomposition of the effect matrix into a series of weighted outer products. This design choice aligns well with the biological assumptions inherent in our application and facilitates the interpretation of results. However, in cases where prior knowledge suggests alternative association structures, such as a modular structure, one can easily modify model (2) by adopting a different decomposition approach, such as a stochastic block model. Moreover, our proposed model can be readily extended to perform heritability analyses for network phenotypes. As a fundamental quantitative genetic

analysis, existing heritability analyses only consider scalar- or vector-variate phenotypes. By adapting our model to this future direction, we could contribute to filling this literature gap and provide valuable insights into the heritability of network-related traits.

References

- Chang, C., Kundu, S., and Long, Q. (2018), “Scalable Bayesian variable selection for structured high-dimensional data,” *Biometrics*, 74, 1372–1382.
- Chen, T., Tan, C., Zhao, H., Constable, T., Yip, S., and Zhao, Y. (2023), “Bayesian subtyping for multi-state brain functional connectome with application on adolescent brain cognition,” *arXiv preprint arXiv:2302.10324*.
- Clark, D. P. and Pazdernik, N. J. (2016), *Biotechnology*, Elsevier, chap. Chapter 8: Genomics and Gene Expression, 2nd ed.
- Desikan, R. S., Sgonne, F., Fischl, B., Quinn, B. T., Dickerson, B. C., Blacker, D., Buckner, R. L., Dale, A. M., Maguire, R. P., Hyman, B. T., Albert, M. S., and Killiany, R. J. (2006), “An automated labeling system for subdividing the human cerebral cortex on MRI scans into gyral based regions of interest,” *NeuroImage*, 31, 968 – 980.
- Elliott, L. T., Sharp, K., Alfaro-Almagro, F., Shi, S., Miller, K. L., Douaud, G., Marchini, J., and Smith, S. M. (2018), “Genome-wide association studies of brain imaging phenotypes in UK Biobank,” *Nature*, 562, 210–216.
- Elsheikh, S. S., Chimusa, E. R., Mulder, N. J., and Crimi, A. (2020), “Genome-wide association study of brain connectivity changes for Alzheimer’s disease,” *Scientific reports*, 10, 1433.
- Eu-Ahsunthornwattana, J., Miller, E. N., Fakiola, M., 2, W. T. C. C. C., Jeronimo, S. M., Blackwell, J. M., and Cordell, H. J. (2014), “Comparison of methods to account for relatedness in genome-wide association studies with family-based data,” *PLoS genetics*, 10, e1004445.
- Ge, T., Reuter, M., Winkler, A. M., Holmes, A. J., Lee, P. H., Tirrell, L. S., Roffman, J. L., Buckner, R. L., Smoller, J. W., and Sabuncu, M. R. (2016), “Multidimensional heritability analysis of neuroanatomical shape,” *Nature Communication*.
- Gelman, A., Rubin, D. B., et al. (1992), “Inference from iterative simulation using multiple sequences,” *Statistical Science*, 7, 457–472.
- Hastie, T., Tibshirani, R., and Friedman, J. (2004), “Optimal predictive model selection,” *Journal of the Royal Statistical Society: Series B (Statistical Methodology)*, 66, 209–233.

- Helgason, A., Yngvadottir, B., Hrafnkelsson, B., Gulcher, J., and Stefánsson, K. (2005), “An Icelandic example of the impact of population structure on association studies,” *Nature genetics*, 37, 90–95.
- Hibar, D. P., Stein, J. L., Renteria, M. E., Arias-Vasquez, A., Desrivières, S., Jahanshad, N., Toro, R., Wittfeld, K., Abramovic, L., Andersson, M., et al. (2015), “Common genetic variants influence human subcortical brain structures,” *Nature*, 520, 224–229.
- Hu, W., Pan, T., Kong, D., and Shen, W. (2021), “Nonparametric matrix response regression with application to brain imaging data analysis,” *Biometrics*, 77, 1227–1240.
- Jahanshad, N., Rajagopalan, P., Hua, X., Hibar, D. P., Nir, T. M., Toga, A. W., Jack Jr, C. R., Saykin, A. J., Green, R. C., Weiner, M. W., et al. (2013), “Genome-wide scan of healthy human connectome discovers SPON1 gene variant influencing dementia severity,” *Proceedings of the National Academy of Sciences*, 110, 4768–4773.
- Kang, H. M., Sul, J. H., Service, S. K., Zaitlen, N. A., Kong, S.-y., Freimer, N. B., Sabatti, C., and Eskin, E. (2010), “Variance component model to account for sample structure in genome-wide association studies,” *Nature genetics*, 42, 348–354.
- Kong, D., An, B., Zhang, J., and Zhu, H. (2019), “L2RM: Low-rank linear regression models for high-dimensional matrix responses,” *Journal of the American Statistical Association*.
- Li, F. and Zhang, N. R. (2010), “Bayesian variable selection in structured high-dimensional covariate spaces with applications in genomics,” *Journal of the American statistical association*, 105, 1202–1214.
- Li, Z., Wang, D., Liao, H., Zhang, S., Guo, W., Chen, L., Lu, L., Huang, T., and Cai, Y.-D. (2022), “Exploring the genomic patterns in human and mouse cerebellums via single-cell sequencing and machine learning method,” *Frontiers in Genetics*, 13, 857851.
- Lyons-Warren, A. M., Wangler, M. F., and Wan, Y.-W. (2022), “Cluster analysis of Short Sensory Profile data reveals sensory-based subgroups in autism spectrum disorder,” *International Journal of Molecular Sciences*, 23, 13030.
- Park, T. and Casella, G. (2008), “The bayesian lasso,” *Journal of the American Statistical Association*, 103, 681–686.
- Polanco, J., Reyes-Vigil, F., Weisberg, S. D., Dhimitruka, I., and Brusés, J. L. (2021), “Differential spatiotemporal expression of type I and type II cadherins associated with the segmentation of the central nervous system and formation of brain nuclei in the developing mouse,” *Frontiers in Molecular Neuroscience*, 14, 633719.
- Ramasamy, A., Trabzuni, D., Guelfi, S., Varghese, V., Smith, C., Walker, R., De, T., Robert, U. B. E. C. H. J. R. M. T. D. G. S. W. M. E. R. A. F. P. . S. C. W., Coin, L., et al. (2014a), “Genetic variability in the regulation of gene expression in ten regions of the human brain,” *Nature neuroscience*, 17, 1418–1428.
- Ramasamy, V. K., Risacher, S. L., Nho, K., Kim, S., Swaminathan, S., Shen, L., Foroud, T. M., Hakonarson, H., Huentelman, M. J., Aisen, P. S., and et al. (2014b), “APOE and BCHE as modulators of cerebral amyloid deposition: a florbetapir PET genome-wide association study,” *Molecular psychiatry*, 19, 351–357.

- Rivero, O., Sich, S., Popp, S., Schmitt, A., Franke, B., and Lesch, K.-P. (2013), “Impact of the ADHD-susceptibility gene CDH13 on development and function of brain networks,” *European Neuropsychopharmacology*, 23, 492–507.
- Shen, L. and Thompson, P. M. (2020), “Brain Imaging Genomics: Integrated Analysis and Machine Learning,” *Proceedings of the IEEE*, 108, 125–162.
- Simon, N., Friedman, J., Hastie, T., and Tibshirani, R. (2013), “A sparse-group lasso,” *Journal of computational and graphical statistics*, 22, 231–245.
- Stingo, F. C., Chen, Y. A., Tadesse, M. G., and Vannucci, M. (2011), “Incorporating biological information into linear models: A Bayesian approach to the selection of pathways and genes,” *The annals of applied statistics*, 5.
- Treutlein, J. and Rietschel, M. (2011), “Genome-wide association studies of alcohol dependence and substance use disorders,” *Current psychiatry reports*, 13, 147–155.
- Van Essen, D. C., Smith, S. M., Barch, D. M., Behrens, T. E., Yacoub, E., Ugurbil, K., Consortium, W.-M. H., et al. (2013), “The WU-Minn human connectome project: an overview,” *Neuroimage*, 80, 62–79.
- Wang, K.-S., Liu, X., Zhang, Q., Pan, Y., Aragam, N., and Zeng, M. (2011), “A meta-analysis of two genome-wide association studies identifies 3 new loci for alcohol dependence,” *Journal of psychiatric research*, 45, 1419–1425.
- Wang, L., Lin, F. V., Cole, M., and Zhang, Z. (2021), “Learning clique subgraphs in structural brain network classification with application to crystallized cognition,” *NeuroImage*, 225, 117493.
- Wang, Y. and Guo, Y. (2020), “Locus: A novel decomposition method for brain network connectivity matrices using low-rank structure with uniform sparsity,” *arXiv preprint arXiv:2008.08915*.
- Zhang, J., Sun, W. W., and Li, L. (2020), “Mixed-effect time-varying network model and application in brain connectivity analysis,” *Journal of the American Statistical Association*, 115, 2022–2036.
- (2023), “Generalized connectivity matrix response regression with applications in brain connectivity studies,” *Journal of Computational and Graphical Statistics*, 32, 252–262.
- Zhang, Z., Descoteaux, M., Zhang, J., Girard, G., Chamberland, M., and Dunson, D. (2018), “Mapping Population-based Structural Connectomes,” *NeuroImage*, 172, 130 – 145.
- Zhao, B., Li, T., Yang, Y., Wang, X., Luo, T., Shan, Y., Zhu, Z., Xiong, D., Hauberg, M. E., Bendl, J., et al. (2021a), “Common genetic variation influencing human white matter microstructure,” *Science*, 372, eabf3736.
- Zhao, B., Zhang, J., Ibrahim, J., Luo, T., Santelli, R., Li, Y., Li, T., Shan, Y., Zhu, Z., Zhou, F., Liao, H., Nichols, T., and Zhu, H. (2021b), “Large-scale GWAS reveals genetic architecture of brain white matter microstructure and genetic overlap with cognitive and mental health traits (n= 17,706),” *Molecular psychiatry*, 26, 3943–3955.

- Zhao, Y., Chang, C., Zhang, J., and Zhang, Z. (2023), “Genetic underpinnings of brain structural connectome for young adults,” *Journal of the American Statistical Association*, 1–15.
- Zhao, Y., Li, T., and Zhu, H. (2022), “Bayesian sparse heritability analysis with high-dimensional neuroimaging phenotypes,” *Biostatistics*, 23, 467–484.
- Zhong, S., Wei, L., Zhao, C., Yang, L., Di, Z., Francks, C., and Gong, G. (2021), “Interhemispheric relationship of genetic influence on human brain connectivity,” *Cerebral Cortex*, 31, 77–88.
- Zhou, X. and Stephens, M. (2012), “Genome-wide efficient mixed-model analysis for association studies.” *Nature Genetics*, 44.